DNA Nanotechnology

DOI: 10.1002/anie.201206253

Quantum-Dot Fluorescence Lifetime Engineering with DNA Origami Constructs**

*Seung Hyeon Ko, Kan Du, and J. Alexander Liddle**

The ability to organize nanostructures of disparate types and materials—such as metal nanoparticles and semiconductor quantum dots—is challenging but essential for the creation of novel materials and devices. Metal nanoparticles (NPs) have interesting individual plasmonic properties and can be organized to exhibit useful collective responses.[1] Quantum dots (Qdots) provide a powerful means to optically access the nanoscale. Bringing the two together in a well-controlled manner can create structures with interesting properties such as fluorescence enhancement/quenching[2] and high efficiency Förster resonance energy transfer.[3] It also has been an area of intense study, both theoretical and experimental, for a wide range of applications including photodetectors,[4] optical modulators[5] and nanoscale lasers.[6] In particular, changing the fluorescence intensity and lifetime of Qdots, when proximate to metal NPs can be used in sensing applications because of the strong distance dependence of the interaction between the Qdots and the ability to engineer the properties (e.g. size, absorbance/emission spectrum) of the individual components over wide ranges.

Numerous strategies have been used to connect and control the distance between Qdots and NPs with nanometer precision.[2,3,7–9] The structures used previously, however, exhibit a limited persistence length (about 50 nm), making the construction of complex geometries required for eventual use in real devices challenging. DNA origami[10] offers a platform with significant advantages: a more rigid scaffold to organize various moieties, increased geometrical complexity, no need to control the stoichiometry of the spacer per NP, and more control over distances.[11] We have therefore chosen to exploit DNA origami for this purpose. We have developed a novel, flexible approach to fluorescence lifetime engineering of CdSe/ZnS (core/shell) Qdots by controlling their coupling to adjacent gold nanoparticles (AuNPs) at geometrically different locations on the DNA origami. To examine these templates in their native state in solution, we use a three-dimensional (3D), real-time, single-particle tracking system. We determine the influence of AuNPs on the Qdot fluorescence lifetime by systematically varying the location, number, and size of AuNPs as well as the interparticle distance and spectral overlap between AuNPs and Qdots. The DNA origami template serves as a programmable nano-pegboard for heterogeneous integration of Qdots and AuNPs wherein complex geometries are created by using modified staple strands on the DNA origami to capture specific nanoparticles (Figure 1). Herein, we manipulate and control the average photon count rate and lifetime of Qdots by varying the geometrical configuration of Qdot–AuNP conjugates on DNA origami and observe good agreement between theory and measurement.

Solution-based measurements are important, because they provide insight into how the templates will behave in a biological environment. The single-particle tracking system enables us to follow the 3D motion of individual diffusing

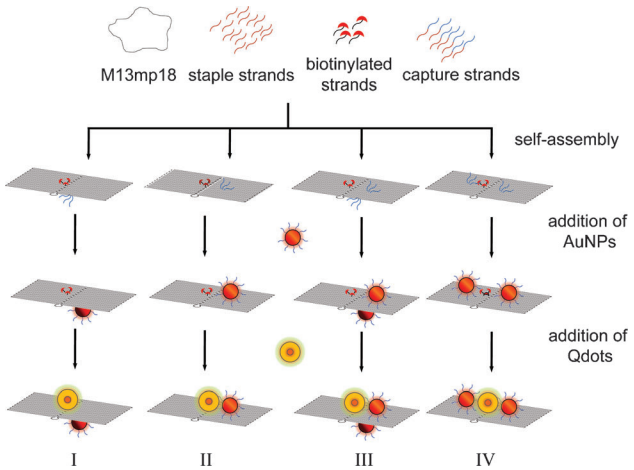

Figure 1. Fabrication process of Qdot–AuNP conjugates on DNA origami templates. Each group of three biotin-conjugated staple strands and triple sticky-end capture strands is located at predetermined binding sites to capture streptavidin-conjugated Qdots and DNA-functionalized AuNPs, respectively. The estimated interparticle distances of Qdots and AuNPs of 15 nm diameter are (15.0 ± 1.1) nm for the same side (II, III, and IV) and (17.6 ± 1.1) nm for the opposite side (I and III).

[*] Dr. S. H. Ko,[+] K. Du,[+] Dr. J. A. Liddle
Center for Nanoscale Science and Technology
National Institute of Standards and Technology
Gaithersburg, MD 20899 (USA)
E-mail: liddle@nist.gov
Dr. S. H. Ko,[+] K. Du[+]
Maryland Nanocenter, University of Maryland
College Park, MD 20742 (USA)
[+] These authors contributed equally to this work.

[**] Dr. S. H. Ko and Dr. K. Du acknowledge support under the Cooperative Research Agreement between the University of Maryland and the National Institute of Standards and Technology Center for Nanoscale Science and Technology, award number 70NANB10H193, through the University of Maryland. The authors are grateful to Dr. H. Lezec and Dr. G. M. Gregg for helpful advice. The authors thank Dr. V. Szalai for helpful discussions and helping with the fluorimeter and Prof. A. Agrawal for comments. The authors also thank Dr. H. Yoon and Dr. J. Schumacher for helping with SEM imaging and Dr. T. Lam for TEM imaging.

Supporting information for this article is available on the WWW under http://dx.doi.org/10.1002/anie.201206253.

fluorescent species in solution over an extended (up to 100 s) period of time (see Figure S1 in the Supporting Information), while detecting the emitted photons with a single-photon-counting Si-avalanche photodiode. The long tracking time significantly improves the signal-to-noise ratio (SNR) which, combined with the single-photon detectors, enables us to measure photon antibunching at mean fluorescence rates as low as 20 kHz.[12] Tracking freely diffusing particles permits noninvasive monitoring of individual DNA origami in buffer solution, in contrast to other measurements that typically employ surface-immobilized DNA origami.[11] Additionally, since single-particle tracking measures diffusion coefficients, we can differentiate between species with different hydrodynamic radii. This property, in conjunction with the fact that the technique is only sensitive to fluorescent particles, means that purification is unnecessary and that concentrations of Qdot as low as about 10^{-12} mol L^{-1} (1 pM) can be used.

To organize AuNPs and Qdots into different geometrical configurations, we use rectangular DNA origami, 70 nm × 100 nm, as a template and modified staple strands at predefined positions extending from either side of the origami. The use of both sides, "up" and "down", provides more flexibility in controlling the location of a nanoparticle. "Up" staple ends are made by shifting each end by five nucleotides at the 3′-end, giving an extra half helical turn (assuming 10.5 bases per turn of B-form helices).[13] Binding locations for AuNPs and Qdots are created by incorporating three hybridizing staple strands or three biotin-modified strands into the origami template, respectively, according to the desired design. AuNPs of 10, 15, and 20 nm diameter (Figure S2) were conjugated with single strands of T18, which were dithiolated at the 5′-end, and further backfilled with thiolated mPEG (methoxypoly(ethylene glycol), molecular weight: 356.5) to fully cover the surface of the AuNPs and avoid aggregation of the AuNPs at the high concentration of Mg^{2+} needed for DNA origami hybridization. We integrated two different Qdots with the DNA origami, with emission spectra centered at 585 and 605 nm, respectively (designated as Qdot 585 or Qdot 605). The Qdots have an approximate diameter of 20 nm, comprising of semiconductor core (3 to 4 nm), a polymer coating, and streptavidins (an average of five to ten molecules). Streptavidin-coated Qdots bind with high (> 90 %) yield to the biotinylated staple strands.[14] We constructed four different configurations of AuNPs and Qdots on DNA origami using both sides of the origami template (Figure 1), by mixing the Qdot solution with the preassembled AuNP–origami template solutions at a stoichiometry of 1:2, and incubating overnight at RT. An excess of AuNP–origami templates minimizes free Qdots. These samples were used without further purification.

Fluorescence lifetimes (τ_f) of the Qdots were measured by performing photon-correlation measurements on each tracked Qdot and analyzing the photon antibunching behavior.[15] CdSe/ZnS Qdots are two-level emitters and the fluorescence exhibits photon antibunching on time scales comparable to the fluorescence lifetime.[15] The probability of detecting two photons simultaneously emitted from a single Qdot is zero, because a finite amount of time is need to cycle the Qdot between the ground and excited states. Photon antibunching is clearly quantified using the second-order photon correlation function in Equation (1):

$$g^2(\tau) = \frac{\langle f(t,t+\tau)\rangle}{\langle f(t)\rangle^2} = \left\{1 - \alpha\exp\left[-\left(\Gamma_e + \tau_f^{-1}\right)|\tau|\right]\right\} g_0^2(\tau) \qquad (1)$$

where $\langle f(t,t+\tau)\rangle$ is the probability of detecting photons between time t and $t+\tau$, Γ_e is the excitation rate (proportional to laser intensity), τ_f is the fluorescence lifetime, α is the depth of the antibunching dip, and $g_0^2(\tau)$ is the correlation function for all other processes affecting the fluorescence statistics. Quantitative measurements of Qdot fluorescence lifetimes were made by measuring $g^2(\tau)$ as a function of the laser power for about 150 templates of each design and applying a simple linear fit.[15]

Figure 2 shows an example of measurement results of antibunching rise rates ($\Gamma = \Gamma_e + \tau_f^{-1}$) with Qdot 585, which has a 15 nm AuNP on the other side of the DNA origami. A total number of 149 Qdots were measured at different laser

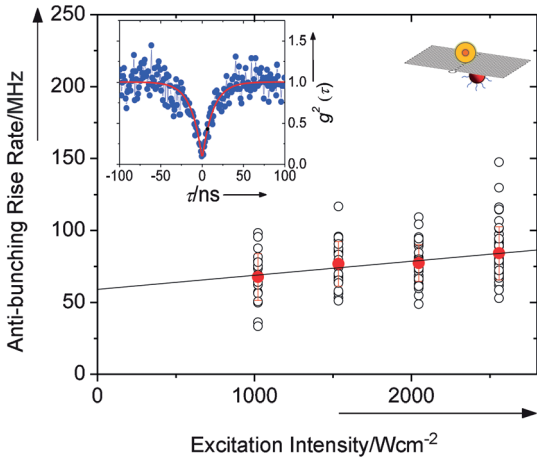

Figure 2. Antibunching rise rates (open circles) of 149 tracked particles of Qdot–AuNP conjugates on DNA origami (Qdot 585, 15 nm AuNP) were measured as a function of laser intensity. Linear fit of the mean values (red dot) gives a lifetime $\tau_f = (17.0 \pm 1.3)$ ns. Inset shows $g^2(\tau)$ (blue dots) of one tracked particle with a fit (red line) to Equation (1). Data for different designs of Qdot–AuNP conjugates on DNA origami are provided in Figure S3.

intensities. A linear fit of the mean values (red dot) indicates that the lifetime τ_f is (17.0 ± 1.3) ns. The inset shows one typical $g^2(\tau)$ plot (blue dots) with a dip centered at $\tau = 0$. A fit (red line) to Equation (1) indicates a rise rate, $\Gamma = 76$ MHz, and antibunching dip, $\alpha \approx 1$, which demonstrates that the fluorescence is from a single Qdot.[16] The variation in rise rates is primarily due to the lifetime heterogeneity within the sample, and not due to a poor SNR (signal-to-noise ratio in our measurement is around 80).[15]

Although analysis of AFM and SEM images (Figures S4 and S5) indicates that the yields of the desired templates are high (> 80 %), it is important to verify that the observed spread in antibunching rise times, and hence lifetime, comes from variations within a particular structure, and not from a mixture of different species. The measured data are well

fitted by single Gaussian functions (Figure S6), lending support to this hypothesis. We note that single-particle measurements are particularly useful in this regard, compared to ensemble lifetime measurements where samples with heterogeneous lifetime distributions can be challenging to analyze.[17]

We determined the influence of AuNPs on Qdot fluorescence lifetime and emission rate by measuring a series of Qdot–AuNP conjugates on DNA origami templates with different geometries. Figure 3 shows the measured average fluorescence lifetime and photon count rate of Qdots with AuNPs in six different configurations. The DNA origami itself does not affect the average lifetime or the fluorescence photon count rate of individual Qdots. However, both of these quantities decrease as the interparticle distance, d, (center of the Qdot to the metal surface of the AuNP) between the AuNPs and Qdots decreases (compare design I vs. design II) or the number of AuNPs increases (compare design II vs. design IV). This dependence on the placement and number of adjacent AuNPs indicates that the lifetime of Qdots can be engineered precisely over a large range.

By using AuNPs of different diameters bound at fixed locations relative to the Qdots, we investigated the influence of different interparticle distances, d, on the fluorescence lifetime of Qdot 585. Larger AuNPs yielded shorter interparticle spacings. For AuNPs having nominal diameters of 10, 15, and 20 nm, we calculated separations of (17.0 ± 0.8), (15.0 ± 1.1), and (13.2 ± 2.1) nm, respectively (Figure S7 and Table 1). The uncertainties in the separations are a result of the distributions of AuNP sizes, which are determined from TEM measurements (Figure S2). The length of the T4 spacer is 1.4 nm, which may contribute some additional uncertainty in the AuNP position.

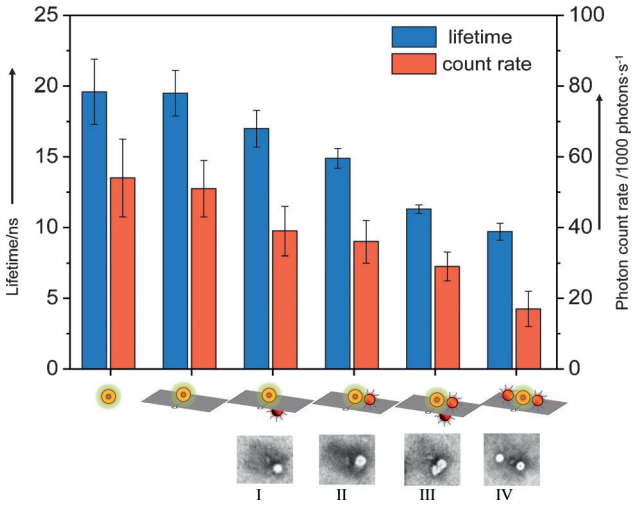

Figure 3. Average photon count rate (right axis) and lifetime (left axis) of Qdot 585 engineered by adjacent 15 nm AuNPs on DNA origami. Error bars are one standard deviation uncertainties derived from the measured distribution of photon count rates and antibunching rise times, respectively. The topographic illustration of each design and its corresponding SEM image are shown at the bottom of the plot. In SEM images, the rectangular shape of DNA origami is visible as a darker gray color and AuNPs and Qdots appear as bright white balls and a small white dot, respectively. Larger area SEM images are available in the Supporting Information (Figure S5).

Table 1: Measured lifetimes and photon count rates for Qdot 585 at different diameters of the AuNPs on the same side of the DNA origami template.

Diameter of AuNPs [nm]	no AuNPs	10	15	20
d [nm][a]	–	17.0 ± 0.8	15.0 ± 1.1	13.2 ± 2.1
lifetime, τ_f [ns]	19.5 ± 1.6	17.5 ± 0.9	14.9 ± 0.7	11.2 ± 1.9
photon count rate[b]	51 ± 8	45 ± 6	36 ± 6	29 ± 5

[a] Spacing between the center of the Qdot and the surface of the AuNP. [b] Measured at about 1000 $W cm^{-2}$ (1000 photons·s^{-1}).

Both the fluorescence lifetime and average photon count rate of Qdot 585 decreased significantly with decreasing interparticle distance, d, (Table 1). We attribute these decreases to excitation energy transfer (EET) from the Qdot to the AuNP.[17,18] In our system, the ratio of d to the AuNP radius lies between 1 and 4. Under these conditions, the normal point dipole approximation that leads to the $1/d^6$ dependence of the lifetime on the distance, characteristic of Förster resonance energy transfer (FRET) is not appropriate and the EET should display a $1/d^n$ distance dependence, with n, itself a function of d, ranging between 3 and 4.[18] Intuitively, this can be understood by noticing that, as the separation between the Qdot and AuNP decreases, the AuNP appears more like an extended metal surface. In the basic point dipole approximation, integration over the surface would lead to an n value of 4.[3b,19] We use a more complete analysis,[20] that includes the effect of high-order multipole terms. At the interparticle distances in our templates, the main effect is on the nonradiative rate, whereas the radiative rate is essentially unaffected. However, this requires a numerical calculation to capture the complex dependence of the Qdot–AuNP interaction.[21] In Figure 4 below we compare calculations of the expected normalized Qdot lifetimes with our measurements. The normalized lifetime of the Qdot, τ_{norm}, is determined from the observed lifetimes given in Equation (2),[20]

$$\tau_{norm} = \tau_{DA}/\tau_D \qquad (2)$$

where τ_{DA} and τ_D are the lifetimes of the donor (Qdot) in the presence and absence of the acceptor (AuNP), respectively.

Comparison of the measured normalized lifetimes with the calculated ones shows excellent agreement (Figure 4). A significant fraction of the variation in normalized lifetime is accounted for simply through the observed distribution in the AuNP diameters: any residual variation is most probably due to small deviations in the actual versus designed particle position. We note that the normalized lifetime is not only sensitive to small variations in the Qdot–AuNP separation, but, at the separations of interest here (Figure S8), becomes more so as the particle size increases. Interestingly, the variation in separation sensitivity with particle size opens up the possibility of tuning the response of a Qdot–AuNP template as a function of particle separation from "hard" to "soft" by combining particles of different sizes and spacings.

We might expect that the normalized photon count rate as a function of particle size would be different from the normalized lifetime, since the former would include not only EET, but also any local field enhancement provided by the

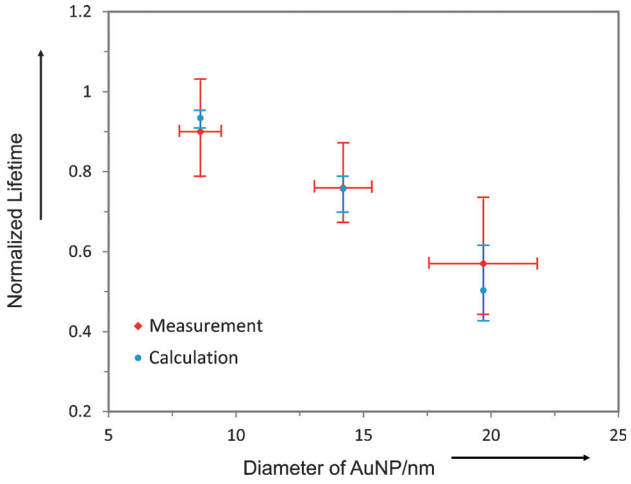

Figure 4. Comparison of calculated and measured normalized lifetime of Qdot 585 with different sizes of AuNPs on the same side of DNA origami (design II). The horizontal error bars for the particle size are one standard deviation (σ), as determined from the TEM measurements of the AuNP diameter, whereas the vertical error bars are one standard deviation in the measured lifetime. The error bars for the calculation are determined by performing the calculation for the range (mean $\pm 1\sigma$) of AuNP sizes observed. The calculation represents the weighted average of the lifetimes given tangential (T) or radial (R) orientations of the Qdot dipole with respect to the AuNP, that is, $(2T+R)/3$.

AuNP. However, a comparison between the normalized count rates and lifetimes (Table S1) shows that there is no significant difference. This is consistent with an analysis by Tanabe,[22] which indicates that, once averaged over all orientations of the incident field, for our values of d to the AuNP radius, minimal field enhancement is expected.

Finally, we find that the degree of spectral overlap between the Qdots and AuNPs correlates with the energy transfer efficiency. Using design II but changing to Qdot 605, which has its emission peak further from the absorption peaks of the AuNPs than Qdot 585 (Figure 5), leads to a decreased

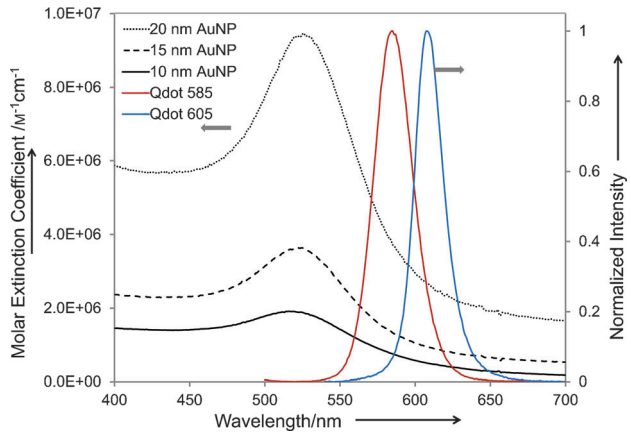

Figure 5. Absorption spectra (left axis) of AuNPs and emission spectra (right axis) of Qdot 585 and Qdot 605 at $\lambda_{excitation}$ of 500 nm. The emission spectra are collected with a long-pass filter with a cutoff of 530 nm.

spectral overlap and a smaller effect on average lifetimes and photon count rates (Table 2).

In conclusion, using single-particle tracking measurements, we have measured the optical response of Qdots in the proximity to AuNPs in a variety of geometries, precisely defined by DNA origami templates. The measurements are made with samples in their native, biologically relevant state in solution. Single-particle tracking measurements allow an unambiguous determination of the source of variation in the optical responses. The ability to exert control over the optical properties (lifetime and photon emission rate) of Qdots is a first step on the way to creating precisely engineered, optically active nanoscale structures that can be used for a wide variety of sensing applications.

Table 2: Measured fluorescence lifetime and average photon count for Qdot 585 and Qdot 605 in the absence and presence (II) of 15 nm AuNP sitting on the same side of the DNA origami.

	Qdot 585		Qdot 605	
	no AuNPs	with AuNP	no AuNPs	with AuNP
lifetime, τ_f [ns]	19.5 ± 1.6	14.9 ± 0.7	10.9 ± 0.3	9.5 ± 0.2
photon count rate r[a]	51 ± 8	36 ± 6	56 ± 12	45 ± 9
$\Delta\tau_f$ [%]	23.6		12.8	
Δr [%]	29.4		19.6	

[a] Measured at about 1000 $W cm^{-2}$ (1000 photons·s^{-1}).

Received: August 3, 2012
Revised: October 26, 2012
Published online: December 23, 2012

Keywords: DNA origami · fluorescence lifetime · nanoparticles · quantum dots · single-molecule studies

[1] A. Kuzyk, R. Schreiber, Z. Fan, G. Pardatscher, E. Roller, A. Högele, F. C. Simmel, A. O. Govorov, T. Liedl, *Nature* **2012**, *483*, 311 – 314.

[2] a) Q. Wang, H. Wang, C. Lin, J. Sharma, S. Zou, Y. Liu, *Chem. Commun.* **2010**, *46*, 240 – 242; b) M. M. Maye, O. Gang, M. Cotlet, *Chem. Commun.* **2010**, *46*, 6111 – 6113; c) Z. Gueroui, A. Libchaber, *Phys. Rev. Lett.* **2004**, *93*, 166108; d) L. Dyadyusha, H. Yin, S. Jaiswal, T. Brown, J. J. Baumberg, F. P. Booy, T. Melvin, *Chem. Commun.* **2005**, 3201 – 3202; e) P. Anger, P. Bharadwaj, L. Novotny, *Phys. Rev. Lett.* **2006**, *96*, 113002; f) D. Guzatov, S. V. Vaschenko, V. V. Stankevich, A. Y. Lunevich, Y. F. Glukhov, S. V. Gaponenko, *J. Phys. Chem. C* **2012**, *116*, 10723 – 10733; g) S. Saini, G. Srinivas, B. Bagchi, *J. Phys. Chem. B* **2009**, *113*, 1817 – 1832.

[3] a) E. Oh, M. Hong, D. Lee, S. Nam, H. C. Yoon, H. Kim, *J. Am. Chem. Soc.* **2005**, *127*, 3270 – 3271; b) T. Pons, I. L. Medintz, K. E. Sapsford, S. Higashiya, A. F. Grimes, D. S. English, H. Mattoussi, *Nano Lett.* **2007**, *7*, 3157 – 3164; c) P. P. Hu, L. Qiang, C. Liu, S. J. Zhen, S. J. Xiao, L. Peng, Y. F. Li, C. Z. Hunag, *Chem. Commun.* **2010**, *46*, 8285 – 8287; d) Y. Kim, Y. Oh, E. Oh, S. Ko, M. Han, H. Kim, *Anal. Chem.* **2008**, *80*, 4634 – 4641; e) H. Liu, G. Liang, E. S. Abdel-Halim, J. Zhu, *Anal. Methods* **2011**, *3*, 1797 – 1801; f) P. C. Ray, A. Fortner, G. K. Darbha, *J. Phys. Chem. B* **2006**, *110*, 20745 – 20748.

[4] a) J. S. White, G. Veronis, Z. F. Yu, E. S. Barnard, A. Chandran, S. H. Fan, M. L. Brongersma, *Opt. Lett.* **2009**, *34*, 686 – 688; b) T. Ishi, J. Fujikata, K. Makita, T. Baba, K. Ohashi, *Jpn. J. Appl. Phys.* **2005**, *44*, L364 – L366.
[5] D. Pacifici, H. J. Lezec, H. A. Atwater, *Nat. Photonics* **2007**, *1*, 402 – 406; D. Pacifici, H. J. Lezec, H. A. Atwater, *Nat. Photonics* **2007**, *1*, 1449 – 1452.
[6] M. A. Noginov, G. Zhu, A. M. Belgrave, R. Bakker, V. M. Shalaev, E. E. Narimanov, S. Stout, E. Herz, T. Suteewong, U. Wiesner, *Nature* **2009**, *460*, 1110 – 1112.
[7] L. Jin, S. Li, B. Kwon, Y. Cho, *J. Appl. Phys.* **2011**, *109*, 124310.
[8] a) O. Kulakovich, N. Strekal, A. Yaroshevich, S. Maskevich, S. Gaponenko, I. Nabiev, U. Woggon, M. Artemyev, *Nano Lett.* **2002**, *2*, 1449 – 1452; b) P. Viste, J. Plain, R. Jaffiol, A. Vial, P. M. Adam, P. Royer, *ACS Nano* **2010**, *4*, 759 – 764; c) X. Ma, H. Tan, T. Kipp, A. Mews, *Nano Lett.* **2010**, *10*, 4166 – 4174; d) D. Ratchford, F. Shafiei, S. Kim, S. K. Gray, X. Li, *Nano Lett.* **2011**, *11*, 1049 – 1054.
[9] Y. Chen, W. Cheng, *WIREs Nanomed. Nanobiotechnol.* **2012**, *4*, 587 – 604.
[10] P. W. K. Rothemund, *Nature* **2006**, *440*, 297 – 302.
[11] a) C. Steinhauer, R. Jungmann, T. L. Sobey, F. C. Simmel, P. Tinnefeld, *Angew. Chem.* **2009**, *121*, 9030 – 9034; *Angew. Chem. Int. Ed.* **2009**, *48*, 8870 – 8873; b) I. H. Stein, V. Schüller, P. Böhm, P. Tinnefeld, T. Liedl, *ChemPhysChem* **2011**, *12*, 689 – 695; c) G. P. Acuna, M. Bucher, I. H. Stein, C. Steinhauer, A. Kuzyk, P. Holzmeister, R. Schreiber, A. Moroz, F. D. Stefani, T. Liedl, F. C. Simmel, P. Tinnefeld, *ACS Nano* **2012**, *6*, 3189 – 3195.
[12] K. Du, J. A. Liddle, A. J. Berglund, *Langmuir* **2012**, *28*, 9181 – 9188.
[13] H. T. Maune, S. Han, R. D. Barish, M. Bockrath, W. A. Goddard III, P. W. K. Rothemund, E. Winfree, *Nat. Nanotechnol.* **2010**, *5*, 61 – 66.
[14] S. H. Ko, G. M. Gregg, J. A. Liddle, *Adv. Funct. Mater.* **2012**, *22*, 1015 – 1023.
[15] K. McHale, A. J. Berglund, H. Mabuchi, *Nano Lett.* **2007**, *7*, 3535 – 3539.
[16] a) B. Lounis, H. A. Bechtel, D. Gerion, P. Alivisatos, W. E. Moerner, *Chem. Phys. Lett.* **2000**, *329*, 399 – 404; b) P. Michler, A. Imamoğlu, M. D. Mason, P. J. Carson, G. F. Strouse, S. K. Buratto, *Nature* **2000**, *406*, 968 – 970.
[17] J. R. Lakowicz, *Principles of Fluorescence Spectroscopy*, 2nd ed., Springer, New York, **2006**, pp. 443 – 448.
[18] S. Bhowmick, S. Saini, V. B. Shenoy, B. Bagchi, *J. Chem. Phys.* **2006**, *125*, 181102.
[19] a) C. S. Yun, A. Javier, T. Jennings, M. Fisher, S. Hira, S. Peterson, B. Hopkins, N. O. Reich, G. F. Strouse, *J. Am. Chem. Soc.* **2005**, *127*, 3115 – 3119; b) T. L. Jennings, M. P. Singh, G. F. Strouse, *J. Am. Chem. Soc.* **2006**, *128*, 5462 – 5467.
[20] A. Moroz, *Opt. Commun.* **2010**, *283*, 2277 – 2287.
[21] Numerical calculations were performed with CRMNT, which can be downloaded from http://www.wave-scattering.com/crmnt.f.
[22] K. Tanabe, *J. Phys. Chem. C* **2008**, *112*, 15721 – 15728.

